Chemical Science

ROYAL SOCIETY OF CHEMISTRY

EDGE ARTICLE

View Article Online
View Journal

Open Access Article. Published on 11 februar 2026. Downloaded on 18-02-2026 21:12:58.
This article is licensed under a Creative Commons Attribution 3.0 Unported Licence.

Check for updates

Cite this: DOI: 10.1039/d5sc08561f

All publication charges for this article have been paid for by the Royal Society of Chemistry

Unlocking spontaneous chiral resolution in silver clusters through steric and anionic control

Jin Liu,[abc] Zi-Ang Nan,*[ab] Qing Li,[abc] Chuan-Qi Shen,[ab] Zuo-Bei Wang,[ab] Fu-Lin Lin,[ab] Ting Chen,[ab] Lu-Yao Liu,[abc] Zhuo-Zhou Xie,[ab] Zhu Zhuo,[ab] Wei Wang[ab] and You-Gui Huang*[abc]

Received 4th November 2025
Accepted 20th January 2026

DOI: 10.1039/d5sc08561f

rsc.li/chemical-science

The spontaneous emergence of chirality from racemic or achiral small molecules and nanoclusters remains a fascinating yet poorly predictable phenomenon. Herein, we report a rational design strategy for achieving spontaneous chiral resolution, as demonstrated through the controlled synthesis of a series of trinuclear silver clusters based on C_3-symmetric tris(2-benzimidazolylmethyl)amine and its derivatives. Our results show that complexes formed by trinuclear clusters bearing sterically demanding ligands and trifluoromethanesulfonate (OTf^-) favor spontaneous chiral resolution, forming homochiral structures due to helical scaffolds from bidirectional intermolecular π···π interactions. In contrast, trinuclear silver clusters bearing ligands with less steric hindrance paired with OTf^- lead to social self-sorting, resulting in racemic crystals. On the other hand, only social self-sorting was observed for the pairing of the trinuclear silver clusters with methanesulfonate (OMs^-). Remarkably, the homochiral structures can be reversibly converted to racemic forms *via* anion exchange, enabling controllable switching between chiral and centrosymmetric polymorphs. The resulting chiral crystals exhibit optical activity and second-harmonic generation (SHG) responses, underscoring their potential for nonlinear optical applications. This work demonstrates that chiral self-sorting can be directed by systematically tuning intermolecular π···π interactions, offering key insights for the rational design of spontaneous resolution systems.

Introduction

Chiral self-sorting refers to the spontaneous organization of racemic or achiral components into homochiral or heterochiral assemblies through chiral recognition.[1–6] This phenomenon not only mimics the stereochemical selection in biological systems but also provides a guiding principle for designing chiral materials and functional devices. Although chirality is crucial across biology,[7–9] asymmetric catalysis,[10–12] and materials science,[13–16] its spontaneous emergence from achiral systems is often considered stochastic. In most cases, obtaining enantiopure crystals still relies on the deliberate introduction of chiral auxiliaries to break the inherent symmetry.[17–20] Although studied for decades, a universal design principle for spontaneous chiral resolution remains elusive, and the process remains largely unpredictable. In solution or soft-matter systems, chiral recognition is usually facilitated by enhancing the steric hindrance of molecular building blocks,[21,22] for example, by the incorporation of flexible chains.[23–27] However, this approach has been largely confined to the formation of amorphous or liquid crystalline phases, and harvesting millimeter-scale chiral single crystals *via* spontaneous resolution remains highly challenging.

Inspired by liquid-crystalline systems, a strategy involving the deliberate enlargement of molecular building blocks *via* rational organic modification has been developed to facilitate spontaneous resolution into chiral single crystals.[28–34] In such systems, symmetry breaking during crystallization is highly dependent on specific intermolecular interactions,[35–38] such as multiple hydrogen bonds and π···π stacking interactions between polycyclic aromatic groups, which are widely recognized as essential for molecular self-recognition. For instance, Yang *et al.* demonstrated that spontaneous symmetry breaking can be achieved by employing multivalent non-covalent interactions to overcome the dipole–dipole interactions that typically favor symmetric antiparallel stacking.[39] Similarly, Jiang *et al.* reported the formation of 2D homochiral helices through orthogonal halogen and hydrogen bonding, leading to effective chiral resolution upon crystallization.[40] Despite these advances, the strategy of deliberately manipulating steric hindrance to direct spontaneous chiral resolution remains a significantly underexplored area.

[a]State Key Laboratory of Structure Chemistry, Fujian Institute of Research on the Structure of Matter, Chinese Academy of Science, Fuzhou, Fujian, 350002, China. E-mail: nanziang@fjirsm.ac.cn; yghuang@fjirsm.ac.cn

[b]Fujian Science & Technology Innovation Laboratory for Optoelectronic Information of China, Fuzhou, Fujian, 350108, China

[c]Xiamen Key Laboratory of Rare Earth Photoelectric Functional Materials, Xiamen Institute of Rare Earth Materials, Haixi Institutes, Chinese Academy of Sciences, Xiamen, Fujian, 361021, China

Open Access Article. Published on 11 februar 2026. Downloaded on 18-02-2026 21:12:58.
This article is licensed under a Creative Commons Attribution 3.0 Unported Licence.

Herein, we report a systematic study on the self-assembly of a series of tripodal ligands (L^1 = tris(2-benzimidazolylmethyl) amine, L^2 = tris(2-fluorobenzimidazolylmethyl)amine, L^3 = tris(2-dimethylbenzimidazolylmethyl)amine, and L^4 = tris(2-naphthimidazolylmethyl)amine with AgOTf and AgOMs. Sterically demanding ligands (L^3, L^4) coordinated with AgOTf produce chiral superstructures, whereas less hindered ligands (L^1, L^2) form racemic crystals. Replacing AgOTf with AgOMs results in racemic products regardless of the ligand. Remarkably, anion exchange enables reversible switching between chiral and racemic polymorphs, highlighting the anion's pivotal role in defining the supramolecular outcome. The resulting chiral crystals are optically and SHG-active, imparting potential for applications in optical materials.

Results and discussion

The reactions of AgOTf or AgOMs with ligands L^1, L^2, L^3, or L^4 in MeOH/acetone in the presence of tetrabutylammonium bromide at room temperature yielded crystals of different trinuclear silver clusters (Tables S1–S3). The ^{1}H NMR spectra for the four ligands are shown in Fig. S1–S4.While the less sterically hindered ligands L^1 and L^2 resulted in racemic complexes $\{[Ag_3L^1{}_2]\cdot(OTf)_3\}$ (**1**) and $\{[Ag_3L^2{}_2]\cdot(OTf)_3\}$ (**2**), the more sterically hindered L^3 and L^4 produced $\{[Ag_3L^3{}_2]\cdot(OTf)_3\}$ (**3a**), $\{[Ag_3L^3{}_2]\cdot(OMs)_2(OTf)\}$ (**3b**), $\{[Ag_3L^4{}_2]\cdot(OTf)_3\}$ (**4a**), and $\{[Ag_3L^4{}_2]\cdot(OMs)_3(H_2O)\}$ (**4b**) (Scheme 1), among which **3a** and **4a** are chiral. Electrospray ionization mass spectrometry (ESI-MS) confirmed the stability of all trinuclear silver clusters in MeOH (Fig. S5–S10). These complexes are further characterized by powder X-ray diffraction (PXRD) (Fig. S11), infrared spectroscopy (IR) (Fig. S12), thermogravimetric analyses (TGA) (Fig. S13), and X-ray photoelectron spectroscopy (XPS) (Fig. S14). In the crystal structures,[41–48] all ligands adopt either a clockwise (*Λ*) or an anticlockwise (*Δ*) conformation (Fig. S15) giving rise to two pairs of potential enantiomers of the trinuclear silver clusters: *ΛΛP*- and *ΔΔM*-$[Ag_3L_2]^{3+}$, *ΛΔP*- and *ΛΔM*-$[Ag_3L_2]^{3+}$ (L represents any of the four ligands of L^1, L^2, L^3, and L^4). Notably, spontaneous chiral resolution occurred during the self-assembly of **3a** and **4a** producing chiral single crystals. Whether spontaneous resolution takes place depends specifically on the substituents of the C_3-symmetric ligands and the choice of silver salt. Therefore, we next sought to elucidate the driving force behind this symmetry-breaking phenomenon.

Since complexes **1** and **2** are isostructural, **1** was selected for detailed crystal structure description. Single-crystal X-ray (SC-XRD) analysis reveals the centrosymmetric space group $R\bar{3}$ for **1** (Table S1). The asymmetric unit contains one Ag^+ ion, two one-third fragments of an L^1 ligand, and one OTf^- anion. The trinuclear $[Ag_3L^1{}_2]^{3+}$ cluster is formed by three Ag^+ ions in a nearly linear geometry (N–Ag–N bond angle: 167.9°) bridged by two L^1 ligands (Fig. S16a). The two ligands adopt opposite twisting directions, clockwise (*Λ*) and anticlockwise (*Δ*), giving rise to a pair of enantiomers *ΛΔP*-$[Ag_3L^1{}_2]^{3+}$ and *ΛΔM*-$[Ag_3L^1{}_2]^{3+}$ (Fig. 1a and b). Clusters of the same handedness are linked by OTf^- *via* hydrogen bonds, forming a chiral *α*-Po network (Fig. S16b and S17). Two such networks of opposite handedness interpenetrate with each other, leading to a racemic structure in which *ΛΔP*-$[Ag_3L^1{}_2]^{3+}$ and *ΛΔM*-$[Ag_3L^1{}_2]^{3+}$ align alternately along the *c* axis (Fig. 1c). In addition to three pairs of intramolecular π-stacked benzimidazolylmethyl arms (centroid–centroid distance of ∼3.71 Å), each $[Ag_3L^1{}_2]^{3+}$ also associates with a neighboring cluster of opposite handedness *via* a weak intermolecular π···π interaction (a centroid–centroid distance of ∼3.91 Å) (Fig. S17d).

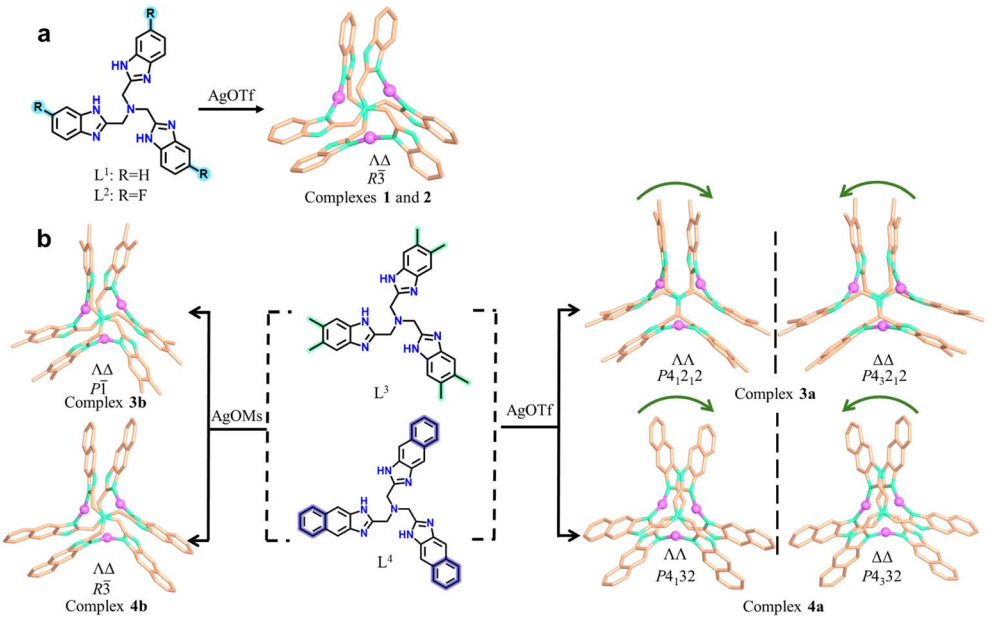

Scheme 1 Formation of the complexes described in this study. (a) Less sterically hindered achiral C_3-symmetric ligands L^1 and L^2 coordinate with AgOTf to form racemic crystals. (b) Sterically demanding ligands L^3 and L^4 coordinate with AgOMs or AgOTf to form either racemic or chiral trinuclear silver cluster complexes.

 © 2026 The Author(s). Published by the Royal Society of Chemistry

Open Access Article. Published on 11 februar 2026. Downloaded on 18-02-2026 21:12:58.
This article is licensed under a Creative Commons Attribution 3.0 Unported Licence.

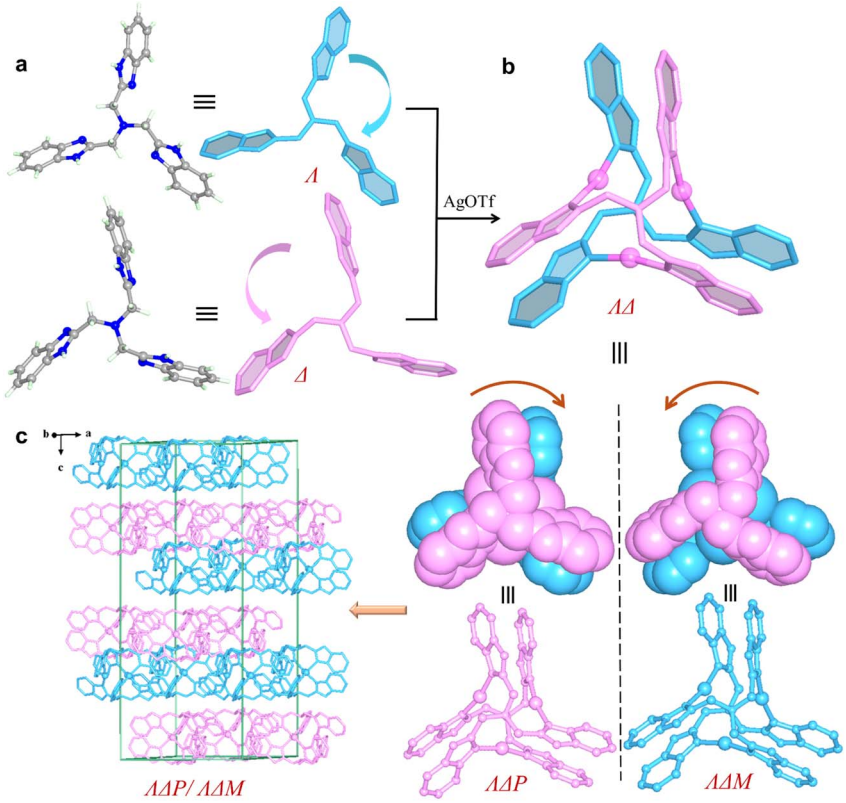

Fig. 1 Racemic crystal structure of **1**. (a) *Λ*- and *Δ*-L^1. (b) *ΛΔP*- and *ΛΔM*-$[Ag_3L^1{}_2]^{3+}$. (c) *ΛΔP*-$[Ag_3L^1{}_2]^{3+}$ and *ΛΔM*-$[Ag_3L^1{}_2]^{3+}$ align alternately along the *c* axis.

To exploit chiral single crystals, we then used more sterically hindered ligands L^3 and L^4 to synthesize silver clusters and successfully obtained chiral complexes **3a** and **4a**. The enantiomers **3a-*P*** and **3a-*M*** crystallize in the chiral tetragonal groups of $P4_12_12$ and $P4_32_12$, respectively (Table S2). We attempted to identify the individual enantiomer *via* macroscopic crystal morphology. Unfortunately, the morphologies of the enantiomeric crystals are nondiscernible because of exposed multiple Miller index facets (Fig. S18). Using **3a-*P*** as a representative, structural analysis shows that its asymmetric unit contains four $[Ag_3L^3{}_2]^{3+}$clusters, two *ΛΛP*-$[Ag_3L^3{}_2]^{3+}$ and *ΛΔP*-$[Ag_3L^3{}_2]^{3+}$, resulting in an enantiomer-pure crystal structure (Fig. 2a and b). In terms of intermolecular π···π interactions, all $[Ag_3L^3{}_2]^{3+}$ clusters utilize each of their three π-stacked arms to associate bidirectionally with two neighboring clusters. As a result, each cluster associates with its six neighbors, forming a porous *α*-Po supramolecular structure with channels along the *c* axis (Fig. S19 and S21). OTf^- anions are located within these channels, with some engaging in NH···O hydrogen bonding with the host framework (Fig. S21). The over three-dimensional (3D) structure is composed of four different types of helical columns formed by dimethylbenzimidazolylmethyl arms (Fig. 2c and S20). Each helical turn comprises 24 π-stacked arms, corresponding to a pitch length of ∼98.16 Å (Fig. 2d).

The enantiomers **4a-*P*** and **4a-*M*** crystallizing in the cubic space groups of $P4_132$ and $P4_332$, respectively, can be clearly identified by their macroscopic crystal morphology (Fig. 3e, S22, and S23), and the structure of **4a-*P*** is briefly described herein (Table S3). Its asymmetric unit contains one-third of the *ΛΛP*-$[Ag_3L^4{}_2]^{3+}$ cluster, and each cluster uses its three pairs of π-stacked naphthimidazolylmethyl arms to bidirectionally associate with its neighboring clusters forming a porous chiral ***srs*** network (Fig. 3 and S24). This chiral network is characteristic of two kinds of small and large helices: smaller helices composed of π-stacked naphthimidazolylmethyl arms and larger helical nanotubes formed by the helical arrangement of the silver clusters (Fig. S24). As observed in **3a**, OTf^- anions are also entrapped within the channels as guest species, stabilized by NH···O hydrogen bonding interactions.

Although isostructural, the four ligands L^1, L^2, L^3, and L^4 feature distinct substitutes, and their coordination with Ag^+ leads to chiral trinuclear Ag^+ clusters of varying configurations. With OTf^-, clusters bearing large steric hindrance ligands are prone to form chiral crystals *via* spontaneous chiral resolution. This process is probably due to narcissistic self-sorting, enabling homochiral clusters to assemble into π-stacked helical columns through intermolecular π···π interactions. The critical role of the counterion is evident, as it dictates the pathway of chiral self-sorting and the final assembled structure.

To illustrate the role of anions in spontaneous chiral resolution, crystals of chiral **3a** were dissolved in methanol containing NaOMs, from which a new racemic complex **3b** was harvested by crystallization. Complex **3b** crystallizes in the centrosymmetric space group $P\bar{1}$, indicating that social self-

Open Access Article. Published on 11 februar 2026. Downloaded on 18-02-2026 21:12:58.
This article is licensed under a Creative Commons Attribution 3.0 Unported Licence.

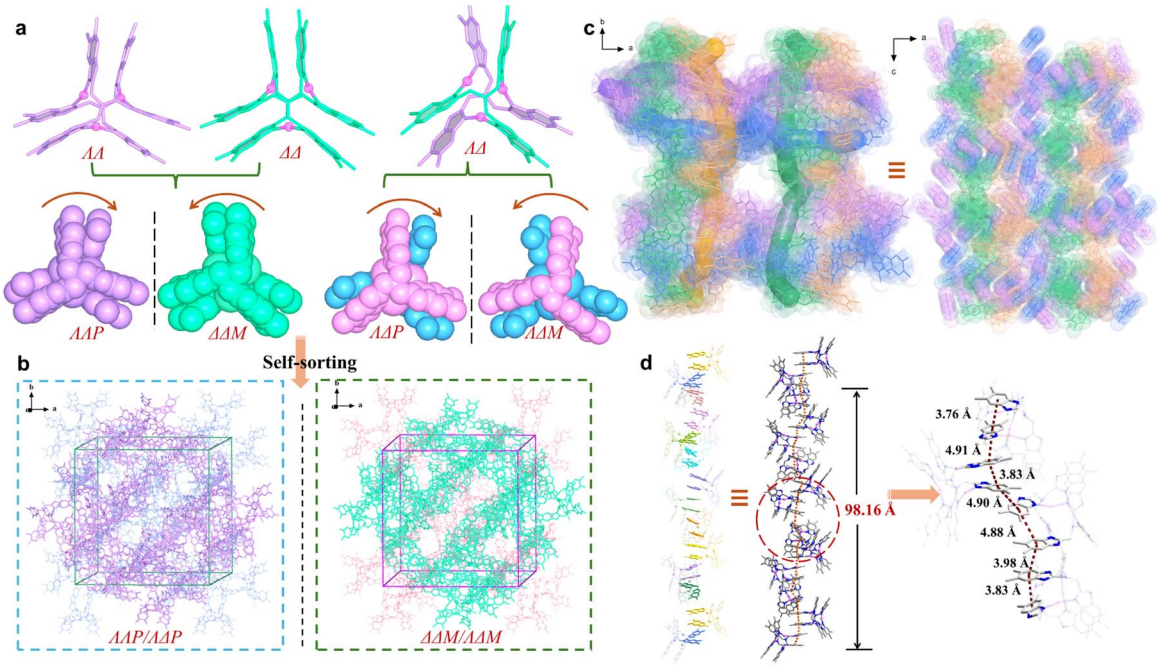

Fig. 2 Crystal structure of **3a**. (a) *ΛΛP*-, *ΔΔM*-, *ΛΔP*-, and *ΛΔM*-$[Ag_3L^3{}_2]^{3+}$ in **3a**-*P* or **3a**-*M*. (b) Narcissistic self-sorting of $[Ag_3L^3{}_2]^{3+}$ forming chiral structures of **3a**-*P* and **3a**-*M*. (c) One of the channels along the *c* axis constructed by quadruple helices in **3a**-*P*. (d) One of the π-stacked helical columns with a pitch of ∼98.16 Å.

sorting occurs during the crystallization. In this crystal structure, $[Ag_3L^3{}_2]^{3+}$ clusters of the same handedness are triple-bridged by OTf^- and OMs^- forming homochiral columns (Fig. S25 and S26). Adjacent heterochiral columns further associate *via* intermolecular π···π interactions, leading to an overall two-dimensional (2D) racemic self-assembly.

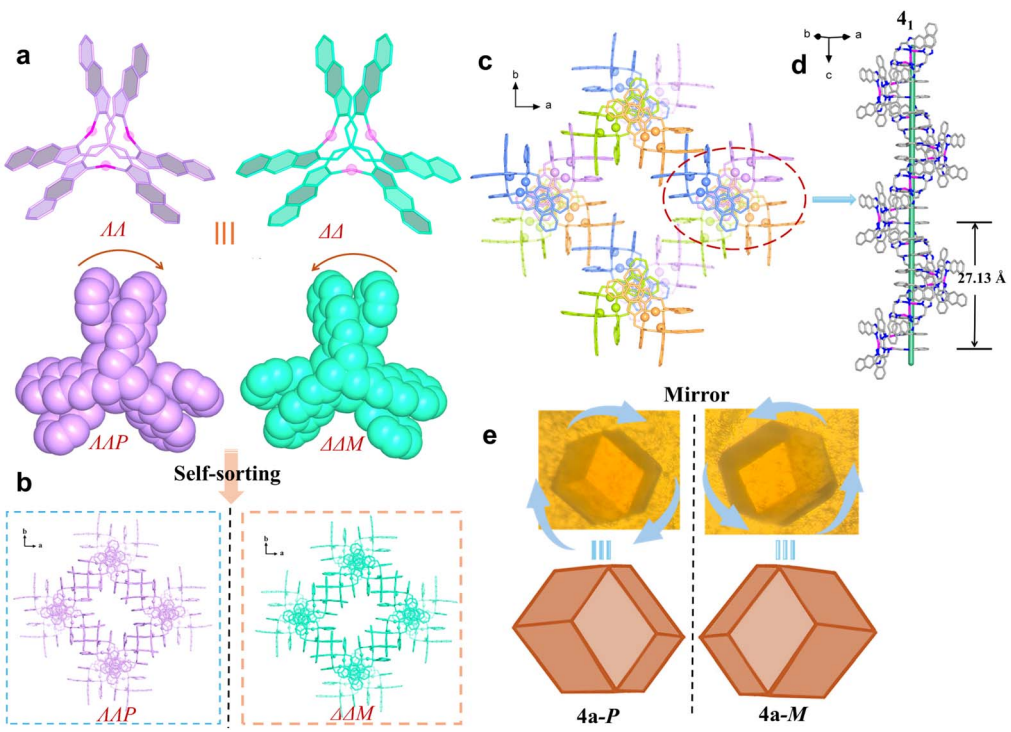

Fig. 3 Crystal structure of **4a**. (a) *ΛΛ*- and *ΔΔ*-$[Ag_3L^4{}_2]^{3+}$ in **4a**-*P* or **4a**-*M*. (b) Narcissistic self-sorting of $[Ag_3L^4{}_2]^{3+}$ forming chiral structures of **4a**-*P* and **4a**-*M*. (c) Chiral *srs* network of **4a**-*P*. (d) 4_1 π-stacked helical column along the *c* axis. (e) The photos of **4a**-*P*/**4a**-*M* crystals.

 © 2026 The Author(s). Published by the Royal Society of Chemistry

Open Access Article. Published on 11 februar 2026. Downloaded on 18-02-2026 21:12:58.
This article is licensed under a Creative Commons Attribution 3.0 Unported Licence.

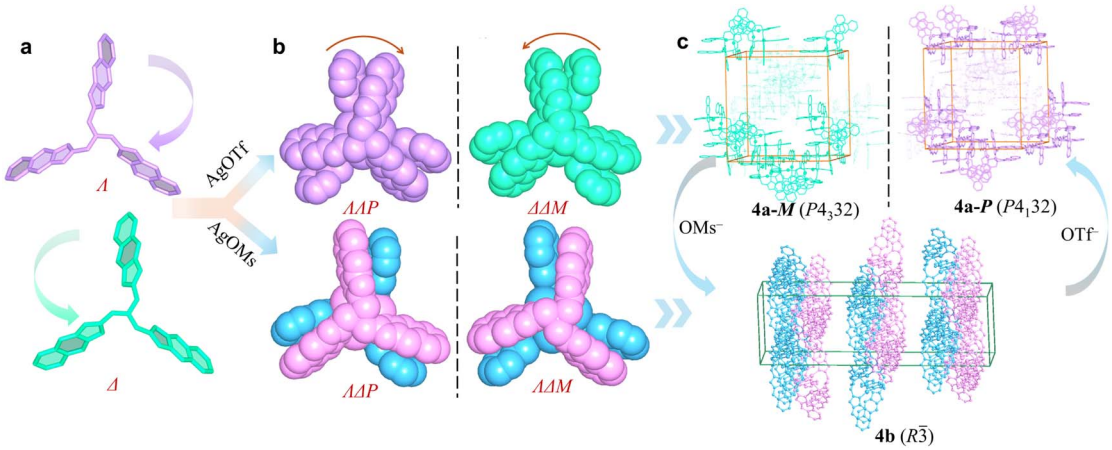

Fig. 4 Anion-induced transition between **4a** and **4b**. (a) *Λ*- and *Δ*-L^4. (b) Two pairs of enantiomers of $[Ag_3L^4{}_2]^{3+}$ (*ΛΛP*- and *ΔΔM*-$[Ag_3L^4{}_2]^{3+}$, *ΛΔP*- and *ΛΔM*-$[Ag_3L^4{}_2]^{3+}$). (c) Anion-induced reversible transition between **4a** and **4b**.

Similarly, the self-assembly between L^4 of AgOMs yields a racemic complex **4b**, which is isostructural to complexes **1** and **2**. In **4b**, $[Ag_3L^4{}_2]^{3+}$ clusters of the same handedness are connected by $[OMs\cdot H_2O]^-$ forming a chiral *α*-Po network (Fig. S27 and S28). Two such *α*-Po networks of opposite handedness interpenetrate *via* intermolecular π···π interactions, resulting in an overall racemic crystal structure. Social self-sorting instead of narcissistic chiral self-sorting occurred during the crystallization of complexes **3b** and **4b**. This difference can be rationalized by the fact that discrete $[Ag_3L^3{}_2]^{3+}$ or $[Ag_3L^4{}_2]^{3+}$ clusters are connected into chiral secondary building units (SBUs) by OMs^- *via* hydrogen bonding. The resulting SBUs tend to undergo socially self-sorting to form racemic structures *via* intermolecular π···π interactions. In contrast, when OTf^- is the counterion, discrete $[Ag_3L^3{}_2]^{3+}$ or $[Ag_3L^4{}_2]^{3+}$ clusters directly engage in narcissistic chiral self-sorting, resulting in the homochiral structures of **3a** and **4a**.

Since counterions are critical to the spontaneous chiral resolution of $[Ag_3L^4{}_2]^{3+}$, the reversible transformation between **4a** and **4b** was further studied. Dissolving crystals of **4a** in methanol containing OMs^-, crystals of **4b** are obtained by crystallization. Conversely, crystals of **4a** (both **4a-*M*** and **4a-*P***) were produced from the solution crystals of **4b** in methanol containing OTf^- (Fig. 4 and S29). This reversible interconversion indicates that reversible Ag^+ coordination and dissociation occur readily in solution, allowing $[Ag_3L^4{}_2]^{3+}$ clusters of diverse configurations to coexist in equilibrium. However, the final self-assembly pathway, either social self-sorting or narcissistic chiral self-sorting, is decisively directed by the nature of the co-crystallizing counterion.

The homochirality of **3a** and **4a** prompted us to study their chiroptical and nonlinear optical properties. Circular dichroism (CD) spectra for **3a-*M***, **3a-*P***, **4a-*M***, and **4a-*P*** were collected from solutions prepared by dissolving a single crystal in 3 mL methanol. Despite that no notable difference in ^{1}H NMR was observed for the pairs of **3a**/**3b** and **4a**/**4b** (Fig. S30–S33), both **3a** and **4a** are CD active. For **3a-*M*** and **3a-*P***, the spectra display a pair of CD signals confirming the enantiopurity of the

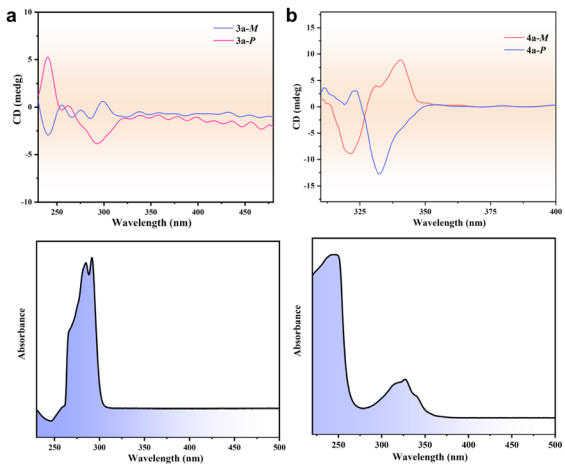

Fig. 5 CD spectra. Circular dichroism (CD) spectra and UV-vis absorption spectra of **3a** (a) and **4a** (b) in methanol.

$[Ag_3L^3{}_2]^{3+}$ clusters in the bulk single crystal. A pair of similar CD signals was observed for the solutions of **4a-*M*** and **4a-*P*** (Fig. 5). Furthermore, both the crystalline samples for **3a** and **4a** show obvious second-harmonic generation (SHG) signals, verifying their non-centrosymmetric crystal structures. The SHG efficiency of **3a** is estimated to be approximately 0.47% of that of KH_2PO_4 (KDP), and that of **4a** is estimated to be approximately 0.38% of KDP under the same experimental conditions. In contrast, the SHG signal from racemic **4b** was negligible. Furthermore, the SHG responses of **4a** and **4b** regenerated *via* anion exchange are consistent with the original samples (Fig. S34). All these results confirm that spontaneous chiral resolution occurs during the crystallization of **3a** and **4a**.

Conclusion

In conclusion, we have systematically investigated how ligand steric hindrance and the anion direct the spontaneous chiral resolution of trinuclear silver clusters based on tripodal ligands

Open Access Article. Published on 11 februar 2026. Downloaded on 18-02-2026 21:12:58.
This article is licensed under a Creative Commons Attribution 3.0 Unported Licence.

L^1, L^2, L^3, and L^4. When OTf^- is the counterion, sterically demanding ligands $[Ag_3L^3{}_2]^{3+}$ and $[Ag_3L^4{}_2]^{3+}$ undergo narcissistic chiral self-sorting, forming homochiral crystals, whereas the less hindered analogues $[Ag_3L^1{}_2]^{3+}$ and $[Ag_3L^2{}_2]^{3+}$ form racemic crystal structures. In contrast, the presence of OMs^- shifts the assembly of $[Ag_3L^3{}_2]^{3+}$ and $[Ag_3L^4{}_2]^{3+}$ toward social self-sorting, resulting in racemic crystals. Remarkably, reversible transformation between the chiral crystal structure and racemic crystal structure of $[Ag_3L^4{}_2]^{3+}$ was achieved *via* anion exchange. The homochirality of the resolved crystals was unambiguously confirmed by circular dichroism (CD) and second-harmonic generation (SHG) measurements.

These findings demonstrate that spontaneous chiral resolution can be rationally controlled through the combined effects of steric hindrance and anionic modulation. Compared with previous examples of chiral recognition, which generally relied on chiral auxiliaries,[17–20] halogen-bonding interactions[40] or specific solvent effects,[49,50] our study achieves enantiopure crystallization through the deliberate design of ligands and careful selection of counterions. These observations can be rationalized by the role of OMs^- in connecting discrete clusters into chiral secondary building units (SBUs) *via* hydrogen bonding, which subsequently favors social self-sorting into racemic crystals through intermolecular $\pi\cdots\pi$ interactions. In comparison, OTf^- allows direct narcissistic self-sorting of discrete $[Ag_3L^3{}_2]^{3+}$ or $[Ag_3L^4{}_2]^{3+}$ clusters *via* intermolecular $\pi\cdots\pi$ interactions. This dual-control strategy demonstrates that spontaneous chiral resolution can be systematically directed through steric and anionic effects that regulate intermolecular interactions, providing an effective approach for the preparation of enantiomerically pure solid-state materials.

Author contributions

Jin Liu synthesized the complexes, performed single-crystal X-ray diffraction studies, carried out other characterization studies, and prepared the initial manuscript draft. Qing Li and Chuan-Qi Shen collected the ESI-MS data. Zuo-Bei Wang performed the XPS data analysis. Fu-Lin Lin measured the SHG responses. Ting Chen, Lu-Yao Liu, Zhuo-Zhou Xie, Zhu Zhuo, and Wei Wang assisted with manuscript preparation. Zi-Ang Nan and You-Gui Huang supervised the project and contributed to manuscript writing. All authors discussed the results and revised the manuscript.

Conflicts of interest

There are no conflicts to declare.

Data availability

The data that support the findings of this study are available from the corresponding author upon reasonable request.

CCDC 2524680–2524681, 2495911–2495914, 2217498, and 2495903 contain the supplementary crystallographic data for this paper.[41–48]

Supplementary information (SI): details of the experimental materials and characterization procedures, and figures providing additional structural, SHG data, and device performance. See DOI: https://doi.org/10.1039/d5sc08561f.

Acknowledgements

This work was supported by the National Natural Science Foundation of China (92261109 and 22371280), the Natural Science Foundation of Xiamen (3502Z202371030), the Natural Science Foundation of Fujian Province (2023J01219), the XMIREM Autonomous Deployment Project of the Recruitment Program of Global Youth Experts (2023GG02 and 2023CX04), the Major Research Plan of the National Natural Science Foundation of China (92361202), the Opening Foundation of State Key Laboratory of Physical Chemistry of Solid Surfaces, Xiamen University (202426), the Self-deployment Project Research Program of Haixi Institutes, Chinese Academy of Sciences (CXZX-2022-GH02), the Youth Innovation Promotion Association of the CAS (2021302), and the Autonomous Deployment Project of the State Key Laboratory of Structure Chemistry (552025311).

References

1 M. A. Mateos-Timoneda, M. Crego-Calama and D. N. Reinhoudt, *Chem. Soc. Rev.*, 2004, **33**, 363–372.
2 M. M. Safont-Sempere, G. Fernández and F. Würthner, *Chem. Rev.*, 2011, **111**, 5784–5814.
3 M. Liu, L. Zhang and T. Wang, *Chem. Rev.*, 2015, **115**, 7304–7397.
4 W. Wang, X. Y. Wang and H. B. Yang, *Chem. Soc. Rev.*, 2016, **45**, 2656–2693.
5 L. J. Chen, H. B. Yang and M. Shionoya, *Chem. Soc. Rev.*, 2017, **46**, 2555–2576.
6 P. Xing and Y. Zhao, *Acc. Chem. Res.*, 2018, **51**, 2324–2334.
7 X. Q. Dou, N. Mehwish, C. L. Zhao, J. Y. Liu, C. Xing and C. L. Feng, *Acc. Chem. Res.*, 2020, **53**, 852–862.
8 M. Z. Sun, L. G. Xu, A. H. Qu, P. Zhao, T. T. Hao, W. Ma, C. L. Hao, C. L. Wen, X. D. Wen, F. M. Colombari, A. F. Moura, N. A. Kotov, C. L. Xu and H. Kuang, *Nat. Chem.*, 2018, **10**, 821–830.
9 C. Y. Wang, H. Y. Zhang, H. Kuang and C. L. Xu, *Matter.*, 2023, **6**, 1752–1781.
10 Y. H. Huang and T. Hayashi, *Chem. Rev.*, 2022, **122**, 14346–14404.
11 F. Li, J. L. Kan, B. J. Yao and Y. B. Dong, *Angew. Chem., Int. Ed.*, 2022, **61**, e202115044.
12 X. Z. Li, J. G. Wu, C. He, Q. T. Meng and C. Y. Duan, *Small*, 2019, **15**, 1970171.
13 G. K. Long, R. Sabatini, M. I. Saidamionov, G. Lakhwani, A. Rasmita, X. G. Liu, E. H. Sargent and W. B. Gao, *Nat. Rev. Mater.*, 2020, **5**, 423–439.
14 W. J. Weng and J. Gao, *J. Am. Chem. Soc.*, 2024, **146**, 13201–13209.

 © 2026 The Author(s). Published by the Royal Society of Chemistry

Open Access Article. Published on 11 februar 2026. Downloaded on 18-02-2026 21:12:58.
This article is licensed under a Creative Commons Attribution 3.0 Unported Licence.

15 L. X. Liu, Y. Yang, S. C. J. Meskers, Q. K. Wang, L. T. Zhang, C. Yang, J. Q. Zhang, L. Y. Zhu, Y. J. Zhang and Z. X. Wei, *Adv. Mater.*, 2023, **35**, 2304627.
16 C. Feng, K. Zhang, B. X. Zhang, L. H. Feng, L. He, C. F. Chen and M. Li, *Angew. Chem., Int. Ed.*, 2025, **64**, e202425094.
17 Q. X. Bai, Y. M. Guan, T. Wu, Y. Liu, Z. R. Zhai, Q. W. Long, Z. Y. Jiang, P. Y. Su, T. Z. Xie, P. S. Wang and Z. Zhang, *Angew. Chem., Int. Ed.*, 2023, **62**, e202309027.
18 M. T. Chen, Z. C. Chen, H. J. Chen, L. Xu, X. J. Kong, L. S. Long and L. S. Zheng, *Sci. China. Chem.*, 2021, **64**, 1698–1702.
19 M. Uno, T. Kojima, N. Kuwamura, N. Yoshinari and T. Konno, *Chem.–Eur. J.*, 2021, **27**, 8358–8364.
20 H. R. Fu, D. D. Ren, K. Zhang, H. Chen, X. Y. Lu, Q. R. Ding and L. F. Ma, *Chin. J. Chem.*, 2024, **42**, 1260–1266.
21 P. C. Shi, G. Y. Chen, Q. Chen, H. T. Wu, S. X. Li, X. Y. Cao, L. L. Yang and Z. Q. Tian, *Chem. Sci.*, 2025, **16**, 5538–5546.
22 S. G. Jiang, L. Zhang and M. H. Liu, *Chem. Commun.*, 2009, **41**, 6252–6254.
23 H. Sasaki, Y. Takanishi, J. Yamamoto and A. Yoshizawa, *J. Soft Matter.*, 2016, **12**, 3331–3339.
24 T. Reppe, S. Poppe, X. Q. Cai, Y. Cao, F. Liu and C. Tschierske, *Chem. Sci.*, 2020, **11**, 5902–5908.
25 H. Takezoe, *Top. Curr. Chem.*, 2012, **318**, 303–330.
26 Z. C. Shen, Y. Q. Jiang, T. Y. Wang and M. H. Liu, *J. Am. Chem. Soc.*, 2015, **137**, 16109–16115.
27 Z. C. Shen, T. Y. Wang and M. H. Liu, *Angew. Chem., Int. Ed.*, 2014, **53**, 13424–13428.
28 X. S. Yan, K. S. Zou, J. L. Cao, X. R. Li, Z. X. Zhao, Z. Li, A. A. Wu, W. Z. Liang, Y. R. Mo and Y. B. Jiang, *Nat. Commun.*, 2019, **10**, 3610.
29 J. T. Yu, Y. Y. Shi, J. L. Sun, J. H. Lin, Z. T. Huang and Q. Y. Zheng, *Sci. Rep.*, 2013, **3**, 1–5.
30 Y. Q. Li, L. Fu, Z. Y. Jiang, E. M. Han, T. Li, Q. X. Bai, T. Z. Xie, Z. Zhang, P. S. Wang and T. Wu, *Angew. Chem., Int. Ed.*, 2025, **64**, e202503833.
31 Y. Zou, X. N. Liu, E. G. Fu and S. D. Zhang, *Angew. Chem., Int. Ed.*, 2023, **62**, e202217225.
32 J. P. Abberley, R. Killah, R. Walker, J. M. D. Storey, C. T. Imrie, M. Salamończyk, C. H. Zhu, E. Gorecka and D. Pociecha, *Nat. Commun.*, 2018, **9**, 228.
33 S. P. Sreenilayam, Y. P. Panarin, J. K. Vij, V. P. Panov, A. Lehmann, P. Marco, M. Prehm and C. Tschierske, *Nat. Commun.*, 2016, **7**, 11369.
34 X. J. Gao, T. T. Wu, F. Y. Ge, M. Y. Lei and H. G. Zeng, *Inorg. Chem.*, 2022, **61**, 18335–18339.
35 J. H. Huang, Z. Y. Wang, S. Q. Zang and T. C. W. Mak, *ACS Cent. Sci.*, 2020, **6**, 1971–1976.
36 J. E. Carpenter and M. Grünwald, *J. Am. Chem. Soc.*, 2020, **142**, 10755–10768.
37 G. M. Upadhyay, H. M. Mande, D. K. Pithadia, R. H. Maradiya and A. V. Bedekar, *Cryst. Growth Des.*, 2019, **19**, 5354–5361.
38 Z. F. Liu, X. Y. Ye, L. H. Chen, L. Y. Niu, W. J. Jin, S. D. Zhang and Q. Z. Yang, *Angew. Chem., Int. Ed.*, 2025, **63**, e202318856.
39 Z. F. Liu, J. H. Ren, P. Li, L. Y. Niu, Q. Liao, S. D. Zhang and Q. Z. Yang, *Angew. Chem., Int. Ed.*, 2023, **62**, e202214211.
40 X. Lin, B. H. Kou, J. L. Cao, P. M. Weng, X. S. Yan, Z. Li and Y. B. Jiang, *Angew. Chem., Int. Ed.*, 2022, **61**, e202205914.
41 CCDC 2524680: Experimental Crystal Structure Determination, 2026, DOI: 10.5517/ccdc.csd.cc2qr49y.
42 CCDC 2524681: Experimental Crystal Structure Determination, 2026, DOI: 10.5517/ccdc.csd.cc2qr4bz.
43 CCDC 2495911: Experimental Crystal Structure Determination, 2026, DOI: 10.5517/ccdc.csd.cc2ps68z.
44 CCDC 2495912: Experimental Crystal Structure Determination, 2026, DOI: 10.5517/ccdc.csd.cc2ps690.
45 CCDC 2495913: Experimental Crystal Structure Determination, 2026, DOI: 10.5517/ccdc.csd.cc2ps6b1.
46 CCDC 2495914: Experimental Crystal Structure Determination, 2026, DOI: 10.5517/ccdc.csd.cc2ps6c2.
47 CCDC 2217498: Experimental Crystal Structure Determination, 2026, DOI: 10.5517/ccdc.csd.cc2dfh6k.
48 CCDC 2495903: Experimental Crystal Structure Determination, 2026, DOI: 10.5517/ccdc.csd.cc2ps60q.
49 X. Q. Liang, Y. Z. Li, Z. Wang, S. S. Zhang, Y. C. Liu, Z. Z. Cao, L. Feng, Z. Y. Gao, Q. W. Xue, C. H. Tung and D. Sun, *Nat. Commun.*, 2021, **12**, 4966.
50 S. B. Wang, W. M. He, Y. J. Cui, Z. Zhou, L. F. Ma and S. Q. Zang, *Nanoscale*, 2023, **15**, 12679–12685.